15th World Congress on Computational Mechanics (WCCM-XV)
8th Asian Pacific Congress on Computational Mechanics (APCOM-VIII)
Virtual Congress: 31 July – 5 August 2022
S. Koshizuka (Ed.)

ISOGEOMETRIC ANALYSIS FOR 3D PRINTED CONCRETE MONOCLINIC TIMOSHENKO BEAM

HUAIKUN CHEN [1], YUCHING WU [2]

[1] Department of Structural Engineering, College of Civil Engineering, Tongji University, Shanghai, China,
2032654@tongji.edu.cn

[2] Department of Structural Engineering, College of Civil Engineering, Tongji University, Shanghai, China,
ycwu@tongji.edu.cn

Key words: *3D-printed concrete, monoclinic material, Timoshenko beam, Non-Uniform Rational B-Spline (NURBS), isogeometric analysis*

Abstract. *Anisotropy is one of the most important characteristics of 3D printed concrete. If material property is only symmetric on one plane, it is called monoclinic material, in which there are totally 13 independent elastic constants. In this paper, 3D printed concrete Timoshenko beam is analysed using isogeometric technique considering the monoclinic material property. Non-uniform Rational B-Spline(NURBS) functions are used as basis functions to integrate with computer aided design data. In addition, several numerical experiments are conducted to verify accuracy of the isogeometric analytical model. It is demonstrated that the proposed method in this paper can be widely used in analyses of 3D printed concrete monoclinic Timoshenko beams.*

1 INTRODUCTION

With the development of economy and the improvement of human living standard, there are more demands for more novel architectural forms, and it is urgent to improve the ability of complex space design. At the same time, as the aging population becomes more and more prominent, the traditional labor-intensive construction method has become more and more difficult to sustain, and the construction industry needs to find new construction methods. Mechanical instead of manual, to achieve automation and intelligent construction, building 3D printing technology provides a good solution to the above problems, the development of building 3D printing technology is the development trend of building structure.

3D printing technology, also known as additive manufacturing technology [1-3], is a technology that uses computer-aided design (CAD) or 3D scanner to obtain data and adopts the method of material layer by layer to make solid parts. Architectural 3D printing technology originated in 1997 from Pegna, an American scholar, who proposed a construction method of free-form components suitable for the layer-by-layer accumulation and selective solidification of cement materials [4]. At present, there are three main 3D printing technologies applied in the field of architecture: contour process [5-6], contour cable-suspended process [7], D-shaped process [8] and concrete printing process [9-11].

One of the most important characteristics of 3D printed concrete materials is anisotropy,

which can be divided into many kinds, including orthotropic material, triangular material, monoclinic material, hexagonal material and triclinic material [12-15]. According to the research of Wu et al. [16], 3D printed concrete materials should be divided into orthotropic materials and monoclinic materials, and the number of independent material parameters should be between 9 and 13. Different from traditional one-piece molding, layer-by-layer accumulation will generate gaps between layers and form weak interfaces, thus leading to anisotropy [17]. Ma et al. believed that the compressive construction process of 3D-printed concrete was the main cause of anisotropy, which would significantly affect the performance of structures under load. The compressive strength and flexural strength of components would decrease, and the bonding ability between interfaces would be significantly weakened [18]. Damage evolution experiments show that there are weak structures between layers or wires, and tensile stress perpendicular to the weak interface between wires is more likely to induce cracks than tensile stress parallel to the weak interface [19]. Through finite element simulation experiments, Xiao et al. explored the influence of interface bonding properties on the anisotropic mechanical behavior of 3D-printed concrete. A finite element model was established to fully consider the interface bonding characteristics and tensile separation laws, and the influence of the corresponding indexes on the compressive strength and flexural strength of concrete was studied by changing the nozzle size, interface bonding strength and concrete properties. The results show that the horizontal shear deformation between the printed fibers can reduce the compressive strength of the 3D printed specimen, and the mid-span tensile strength determines the bending strength of the 3D printed specimen. The number of interfaces, tensile and shear properties of interfaces are the main factors affecting the compression and bending anisotropy of printed monofilaments [20].

Compared with ordinary concrete construction, the mechanical properties of 3D printed concrete are weaker [21-22]. One way to solve the problem is to add short fibers. It is more difficult to carry out numerical analysis on 3D printed concrete model, especially for complex space design, traditional finite element analysis means are more difficult to sustain. Isometric analysis (IGA) method is based on the idea of iso-parametric element of finite element method. Nonuniform rational B-splines (NURBS) are used as basic functions to represent model geometry in computer-aided design. Without changing geometric shape or parameterization, the introduction of geometric error is prevented and the calculation accuracy is improved [23-24]. Isometric analysis realizes the seamless integration of computer aided design (CAD) and finite element method (FEM), which provides an effective solution for the numerical analysis of 3D printed concrete.

2 NONUNIFORM RATIONAL B-SPLINE FUNCTIONS

The spline function can be determined by a set of one-dimensional vectors, which are a set of non-decreasing coordinates in the parameter space, written as $\theta=\{\xi_1, \xi_2, \xi_3,\cdots, \xi_{n+p+1}\}$. $\xi_i \in R$,i is the ith vector, i is the junction index, i =1,2... , n + p+ 1, where p is the degree of the polynomial and n is the number of basis functions used to construct a B-spline curve. $[\xi_i, \xi_{i+p+1}]$ is the support interval of $N_{i,p}$, If nodes are equally spaced in the parameter space, the node vector is uniform. If they are not equally spaced, then the knot vectors are nonuniform. Node values may be repeated, and the multiplicity of nodes is important for the properties of bases.

2.1 B-spline curve

Based on the concept of vector, the basis function is defined as follows.
When p=0,

$$N_{i,0}(\xi)=\begin{cases}1, \text{when} \xi_i \le \xi < \xi \\ 0, others\end{cases} \tag{1}$$

When $p\neq 0$,

$$N_{i,p}(\xi)=\frac{\xi-\xi_i}{\xi_{i+p}-\xi_i}N_{i,p-1}(\xi)+\frac{\xi_{i+p+1}-\xi}{\xi_{i+p+1}-\xi_{i+1}}N_{i,p+1}(\xi) \tag{2}$$

B-spline curves are constructed by linear combinations of B-spline basis functions, just like classical finite element analysis. The vector-valued coefficients of the basis function are called control points. They are similar to node coordinates in finite element analysis.

The function of the B-spline curve is given as

$$C(\xi)=\sum_{i=1}^{n} N_{i,p}(\xi)B_i \tag{3}$$

Where $N_{i,p}(\xi)$ is the basis function and B_i is the control point.

2.2 B-spline surface and block

According to the control points $B_{i,j}$ with i=1,2,3,⋯,n, and j=1,2,3,⋯,m, degree of polynomial p and q, node vector $\theta=\{\xi_1, \xi_2, \xi_3,\cdots, \xi_{n+p+1}\}$、$\vartheta=\{\eta_1, \eta_2, \eta_3,\cdots, \eta_{m+q+1}\}$, B-spline surface can be defined as

$$S(\xi,\eta)=\sum_{i=1}^{n}\sum_{j=1}^{m} N_{i,p}(\xi)M_{j,q}(\eta)B_{i,j} \tag{4}$$

where $N_{i,p}(\xi)$, $M_{j,q}(\eta)$ is the p-order, q-order univariate B-spline basis function.

Similarly, B-spline block is given as

$$S(\xi,\eta,\zeta)=\sum_{i=1}^{n}\sum_{j=1}^{m}\sum_{k=1}^{l} N_{i,p}(\xi)M_{j,q}(\eta)L_{k,r}(\eta)B_{i,j,k} \tag{5}$$

3 MONOCLINIC CONSTITUTIVE RELATION

For the sake of representation, we make $\sigma_1=\sigma_{tt}$, $\sigma_2=\sigma_{nn}$, $\sigma_3=\sigma_{bb}$, $\sigma_4=\sigma_{nb}$, $\sigma_5=\sigma_{tb}$, $\sigma_6=\sigma_{tn}$, and $\varepsilon_1=\varepsilon_{tt}$, $\varepsilon_2=\varepsilon_{nn}$, $\varepsilon_3=\varepsilon_{bb}$, $\varepsilon_4=2\varepsilon_{nb}$, $\varepsilon_5=2\varepsilon_{tb}$, $\varepsilon_6=2\varepsilon_{tn}$.The stress-strain relationship is given as

$$\begin{Bmatrix}\sigma_1\\ \sigma_2\\ \sigma_3\\ \sigma_4\\ \sigma_5\\ \sigma_6\end{Bmatrix}=\begin{bmatrix}C_{11} & C_{12} & C_{13} & C_{14} & C_{15} & C_{16}\\ C_{21} & C_{22} & C_{23} & C_{24} & C_{25} & C_{26}\\ C_{31} & C_{32} & C_{33} & C_{34} & C_{35} & C_{36}\\ C_{41} & C_{42} & C_{43} & C_{44} & C_{45} & C_{46}\\ C_{51} & C_{52} & C_{53} & C_{54} & C_{55} & C_{56}\\ C_{61} & C_{62} & C_{63} & C_{64} & C_{65} & C_{66}\end{bmatrix}\begin{Bmatrix}\varepsilon_1\\ \varepsilon_2\\ \varepsilon_3\\ \varepsilon_4\\ \varepsilon_5\\ \varepsilon_6\end{Bmatrix} \tag{6}$$

where C_{ij} is elastic constant, $C_{ij}= C_{ji}$.

For monoclinic materials, the stress-strain relationship is given as

$$\begin{Bmatrix}\sigma_1\\ \sigma_2\\ \sigma_3\\ \sigma_4\\ \sigma_5\\ \sigma_6\end{Bmatrix}=\begin{bmatrix}C_{11} & C_{12} & C_{13} & C_{14} & 0 & 0\\ C_{21} & C_{22} & C_{23} & C_{24} & 0 & 0\\ C_{31} & C_{32} & C_{33} & C_{34} & 0 & 0\\ C_{41} & C_{42} & C_{43} & C_{44} & 0 & 0\\ 0 & 0 & 0 & 0 & C_{55} & 0\\ 0 & 0 & 0 & 0 & 0 & C_{66}\end{bmatrix}\begin{Bmatrix}\varepsilon_1\\ \varepsilon_2\\ \varepsilon_3\\ \varepsilon_4\\ \varepsilon_5\\ \varepsilon_6\end{Bmatrix} \tag{7}$$

There are 13 independent parameters in the matrix(C_{11}, C_{22}, C_{33}, C_{44}, C_{55}, C_{66}, C_{12}, C_{23}, C_{45}, C_{13}, C_{14}, C_{24}, C_{34})

For orthotropic materials, the stress-strain relationship is given as

$$\begin{Bmatrix}\sigma_1\\ \sigma_2\\ \sigma_3\\ \sigma_4\\ \sigma_5\\ \sigma_6\end{Bmatrix}=\begin{bmatrix}C_{11} & C_{12} & C_{13} & 0 & 0 & 0\\ C_{21} & C_{22} & C_{23} & 0 & 0 & 0\\ C_{31} & C_{32} & C_{33} & 0 & 0 & 0\\ 0 & 0 & 0 & C_{44} & 0 & 0\\ 0 & 0 & 0 & 0 & C_{55} & 0\\ 0 & 0 & 0 & 0 & 0 & C_{66}\end{bmatrix}\begin{Bmatrix}\varepsilon_1\\ \varepsilon_2\\ \varepsilon_3\\ \varepsilon_4\\ \varepsilon_5\\ \varepsilon_6\end{Bmatrix} \tag{8}$$

There are nine independent parameters in the matrix(C_{11}, C_{22}, C_{33}, C_{44}, C_{55}, C_{66}, C_{12}, C_{23}, C_{13}).

For isotropic materials there are only two independent constants($C_{11}=C_{22}=C_{33}=2\mu+\lambda$, $C_{44}=C_{55}=C_{66}=\mu$, $C_{12}=C_{23}=C_{13}=\lambda$, where μ and λ are constants).

4 NUMERICAL EXAMPLES

It is demonstrated that 3D printed structures show monoclinc materials at macro level. Thus, isotropic materials are used for conventional concrete in the following cases, while monoclinic materials are used for 3D printed structures. The properties of isotropic and monoclinic materials selected were derived from the finite element analysis structure of 3D-printed concrete materials by Wu et al. [16]. properties of isotropic materials are shown in table1

.

Table 1: properties of isotropic materials

Elastic coefficient	Values
Young modulus(GPa)	29.17
Poisson's ratio	0.2

The properties of monoclinic materials are shown in Eq.(9), and the The direction of 3D printing is along the beam which is shown in Figure 1

$$\begin{Bmatrix}\sigma_1\\ \sigma_2\\ \sigma_3\\ \sigma_4\\ \sigma_5\\ \sigma_6\end{Bmatrix}=\begin{bmatrix}C_{11} & C_{12} & C_{13} & C_{14} & 0 & 0\\ C_{21} & C_{22} & C_{23} & C_{24} & 0 & 0\\ C_{31} & C_{32} & C_{33} & C_{34} & 0 & 0\\ C_{41} & C_{42} & C_{43} & C_{44} & 0 & 0\\ 0 & 0 & 0 & 0 & C_{55} & 0\\ 0 & 0 & 0 & 0 & 0 & C_{66}\end{bmatrix}\begin{Bmatrix}\varepsilon_1\\ \varepsilon_2\\ \varepsilon_3\\ \varepsilon_4\\ \varepsilon_5\\ \varepsilon_6\end{Bmatrix} \tag{9}$$

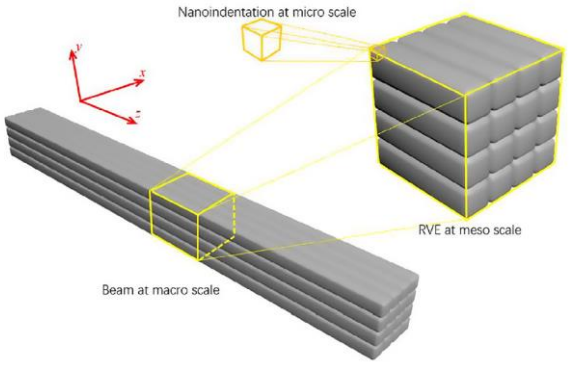

- **Figure 1**: Relationship between constitutive and printing direction

Based on the research results of Al Abadia et al. [25], this paper establishes the material properties of concrete with carbon fiber, Kevlar fiber and glass fiber by VAS method. The component volume of each material can be expressed as follows.

$$V_{concrete} = \frac{V_{concrete}}{V_{coupon}} \tag{10}$$

$$V_{FRP} = \frac{V_{FRP}}{V_{coupon}} \tag{11}$$

where $V_{concrete}$and V_{FRP} represent the volume of concrete and fiber respectively.

According to concrete elastic matrix and FRP fiber elastic matrix, the stiffness matrix of 3D printing material is calculated given as

$$Q = V_{concrete}\bar{Q}_{concrete} + V_{FRP}\bar{Q}_{FRP} \tag{12}$$

$$\bar{Q}_{concrete} = [T]^T Q_{concrete}[T] \tag{13}$$

$$\bar{Q}_{FRP} = [T]^T Q_{FRP}[T] \tag{14}$$

$$Q_{FRP} = \begin{bmatrix} E_1/(1-\nu_{12}\nu_{21}) & \nu_{12}E_2/(1-\nu_{12}\nu_{21}) & 0 \\ \nu_{21}E_2/(1-\nu_{12}\nu_{21}) & E_2/(1-\nu_{12}\nu_{21}) & 0 \\ 0 & 0 & G_{12} \end{bmatrix} \tag{15}$$

$$T = \begin{bmatrix} \cos^2\theta & \sin^2\theta & \sin\theta\cos\theta \\ \sin^2\theta & \cos^2\theta & -\sin\theta\cos\theta \\ \sin\theta\cos\theta & -\sin\theta\cos\theta & \cos^2\theta-\sin^2\theta \end{bmatrix} \tag{16}$$

$\bar{Q}_{concrete}$ 、 $\bar{Q}_{FRP}$ represent the concrete stiffness matrix and fiber stiffness matrix respectively under the overall coordinates, and T represents the transformation matrix.

The properties of carbon fiber, Kevlar fiber and glass fiber are shown in the table 2. The elastic matrix of carbon fiber , Kevlar fiber and glass fiber are shown in Eqs.(17-19).

Table 2. The properties of carbon fiber, Kevlar fiber and glass fiber

Properties	Carbon fiber	Kevlar fiber	Glass fiber
Axial Young modulus E1（Gpa）	85	30	25
Lateral Young modulus E2（Gpa）	26	10	5
shear modulus G12，G23（Gpa）	5	5	1
Poisson's ratio	0.3	0.2	0.2

Elastic matrix of carbon fiber is given as

$$K=\begin{bmatrix} 93.41 & 8.57 & 8.57 & 0 & 0 & 0 \\ 8.57 & 28.57 & 8.57 & 0 & 0 & 0 \\ 8.57 & 8.57 & 28.57 & 0 & 0 & 0 \\ 0 & 0 & 0 & 5 & 0 & 0 \\ 0 & 0 & 0 & 0 & 5 & 0 \\ 0 & 0 & 0 & 0 & 0 & 5 \end{bmatrix} \tag{17}$$

Elastic matrix of Kevlar fiber is given as

$$K=\begin{bmatrix} 31.25 & 2.08 & 2.08 & 0 & 0 & 0 \\ 2.08 & 10.42 & 2.08 & 0 & 0 & 0 \\ 2.08 & 2.08 & 10.42 & 0 & 0 & 0 \\ 0 & 0 & 0 & 5 & 0 & 0 \\ 0 & 0 & 0 & 0 & 5 & 0 \\ 0 & 0 & 0 & 0 & 0 & 5 \end{bmatrix} \tag{18}$$

Elastic matrix of glass fiber is given as

$$K=\begin{bmatrix} 26.04 & 1.04 & 1.04 & 0 & 0 & 0 \\ 1.04 & 5.21 & 1.04 & 0 & 0 & 0 \\ 1.04 & 1.04 & 5.21 & 0 & 0 & 0 \\ 0 & 0 & 0 & 1 & 0 & 0 \\ 0 & 0 & 0 & 0 & 1 & 0 \\ 0 & 0 & 0 & 0 & 0 & 1 \end{bmatrix} \tag{19}$$

4.1 L-shaped beam

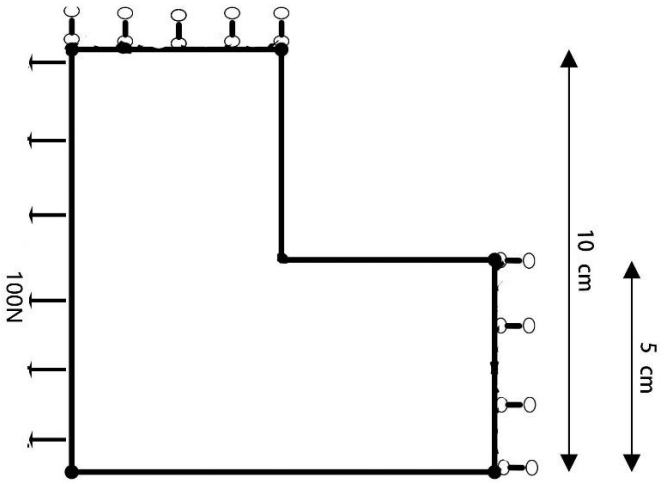

- **Figure 2**: L-shaped beam

The L-shaped beam structure is shown in Figure 2, and the left side is subjected to 100N tensile force. The 3D printing direction is along the L-shaped direction. The use of isotropic materials and monoclinic materials (3D printing) is analyzed respectively. In order to explore the mechanical properties of 3D printed components with adding fibers, the situation of adding fibers was also studied.

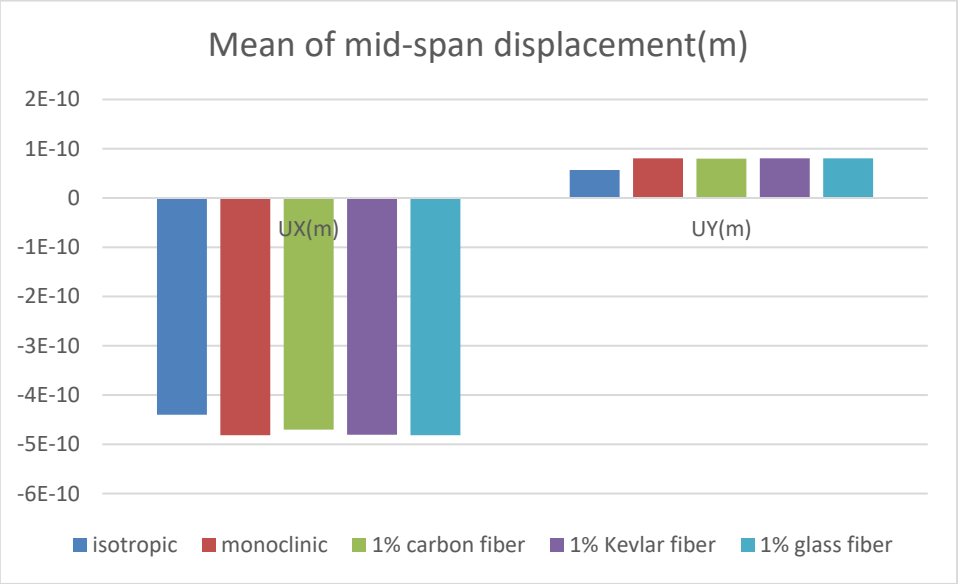

- **Figure 3**: Mean of mid-span displacement

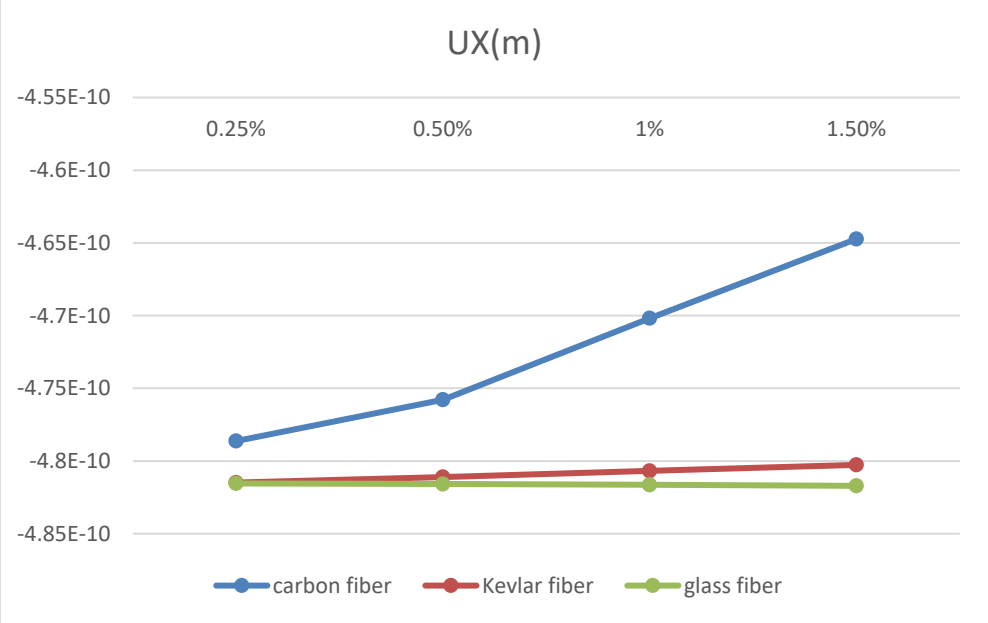

- **Figure 4**: UX at different fiber content

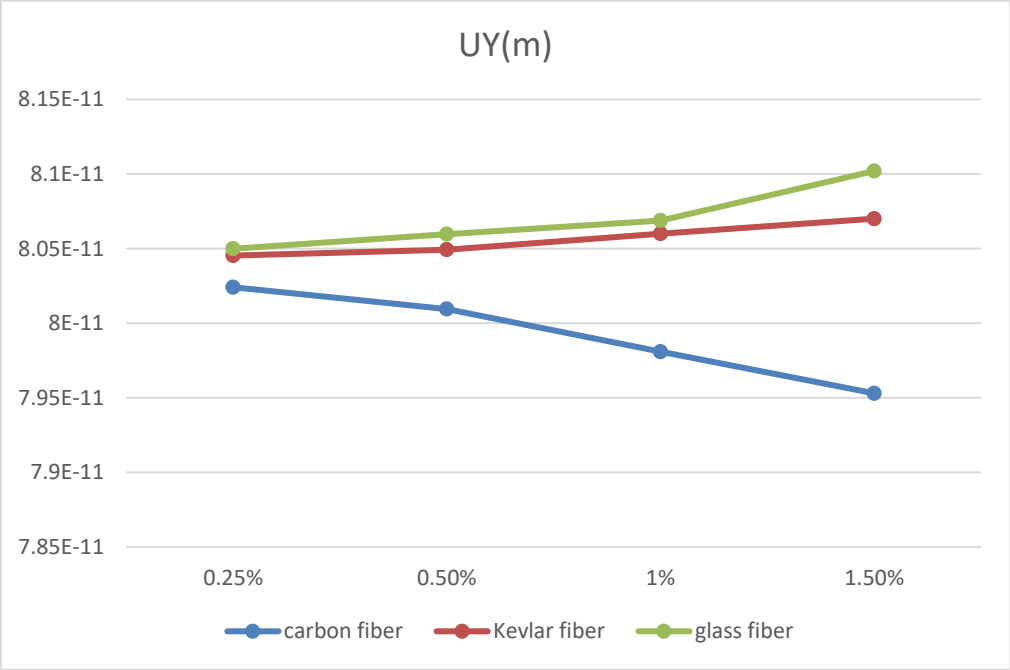

- **Figure 5**: UY at different fiber content

4.2 Quarter circle ring beam

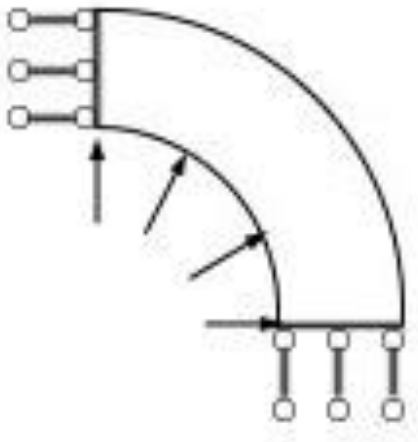

- **Figure 6**: Quarter circle ring beam

The quarter circle ring beam is shown in Fig 6. The inner diameter of the annular beam is 0.3m and the outer diameter is 0.5m. The inner part of the ring is subjected to radial pressure of 1KN. The 3D printing direction is along the circumferential direction.The use of isotropic materials and monoclinic materials (3D printing) is analyzed respectively. In order to explore the mechanical properties of 3D printed components with adding fibers, the situation of adding fibers was also studied.

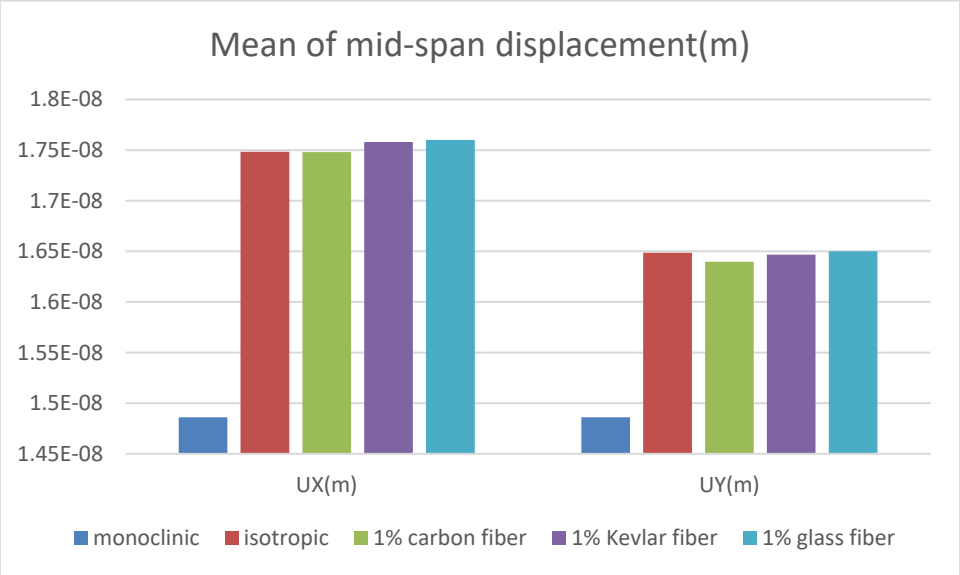

- **Figure 7**: Mean of mid-span displacement

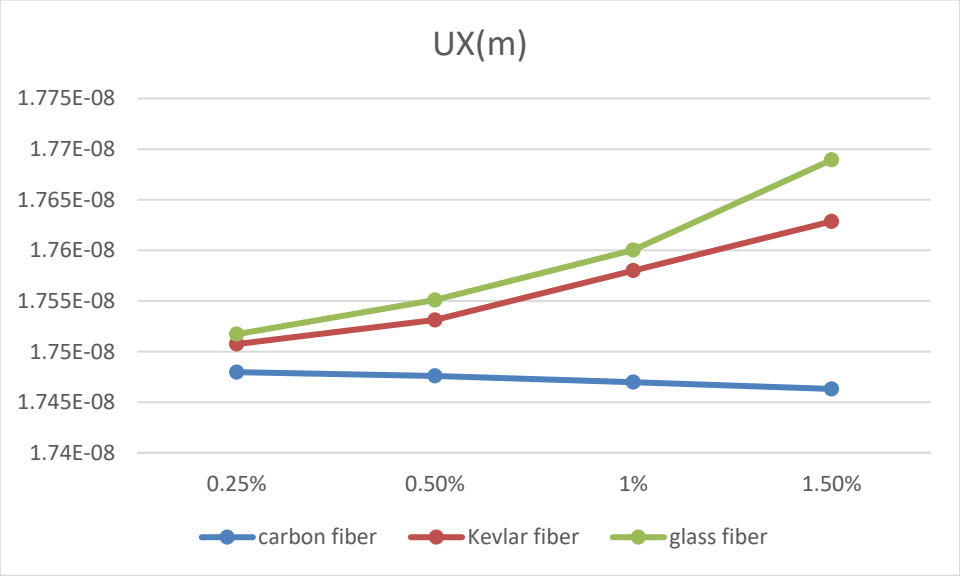

- **Figure 8**: UX at different fiber content

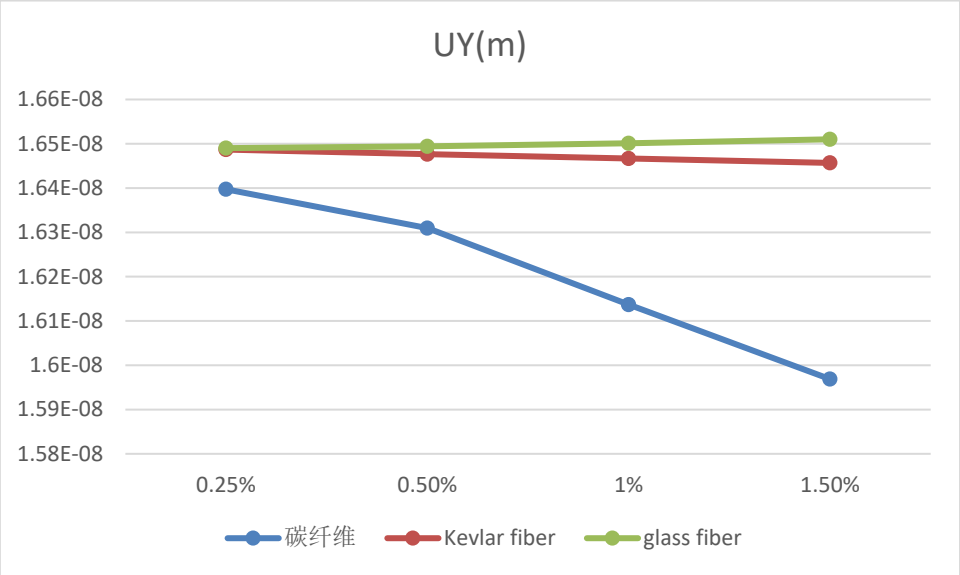

- **Figure 9**: UY at different fiber content

Previous results indicate that in the elastic range the 3D printed concrete beam produces greater deformation than the conventional beam under the same loading. In addition, addition of carbon fiber reduces deformation, while adding Kevlar fiber and glass fiber yields increase of deformation of the beam.

5 CONCLUSIONS

In this paper, isogeometric analysis of 3D printed concrete monoclinic Timoshenko beam is carried out based on Non-Uniform Rational B-Spline functions. It is indicated that the isogeometric approach is superior to conventional finite element method. It is indicated that in the elastic range, deformation of the monoclinic concrete beam is greater than one of the isotropic concrete beam under the same loading. Deflection of concrete beam reinforced with carbon fiber decreases considerably, while one of concrete beam reinforced with Kevlar fiber and glass fiber increases. It is demonstrated that effect of mixing fibers on global structural behavior is significant.

REFERENCES

[1] Gibson I, Rosen D W, Stucker B. Additive manufacturing technologies[M]. New York: Springer, 2014: 1-2.
[2] Mueller B. Additive manufacturing technologies–Rapid prototyping to direct digital manufacturing[J]. Assembly Automation, 2012, 32(2).
[3] Frazier W E. Metal additive manufacturing: a review[J]. Journal of Materials Engineering and Performance, 2014, 23(6): 1917-1928.
[4] Pegna J. Exploratory investigation of solid freeform construction[J]. Automation in construction, 1997, 5(5): 427-437.
[5] Ding L, Xv J, Qin Y. Summary of research and application of 3D printing digital construction technology in architecture [J]. Journal of Civil Engineering and Management, 2015, 32(3): 1-10.
[6] Khoshnevis B, Hwang D, Yao KT, et al. Mega-scale fabrication by contour crafting[J]. International Journal of Industrial and Systems Engineering, 2006, 1(3): 301-320.

[7] Bosscher P, Williams II RL, Bryson LS, et al. Cable-suspended robotic contour crafting system[J]. Automation in construction, 2007, 17(1): 45-55.
[8] Khoshnevis B, Thangavelu M, Yuan X, et al. Advances in contour crafting technology for extraterrestrial settlement infrastructure buildup[C]. AIAA SPACE 2013 Conference and Exposition. 2013: 5438.
[9] Soar R, Andreen D. The role of additive manufacturing and physiomimetic computational design for digital construction[J]. Architectural Design, 2012, 82(2): 126-135.‘
[10] Le TT, Austin SA, Lim S, et al. Mix design and fresh properties for high-performance printing concrete[J]. Materials & Structures, 2012, 45(8): 1221.
[11] Ma GW, Wang L, Ju Y. State-of-the-art of 3d Printing technology of cementitious material-An emerging technique for construction[J]. Science China Technological Sciences, 2018, 61: 475.
[12] Batra RC, Qian LF, Chen LM. Natural frequenciesof thick square plates made of orthotropic, trigonal, monoclinic, hexagonal and triclinic materials, Journal of Sound and Vibration 270 (2004) 1074–1086.
[13] Bahrami K, Afsari A, Janghorban M, Karami B. Static analysis of monoclinic plates via a three-dimensional model using differential quadrature method, Structural Engineering and Mechanics 72 (2019) 893-901.
[14] Ferreira AJM, Fasshauer GE, Batra RC. Natural frequencies of thick plates made of orthotropic, monoclinic, and hexagonal materials by a meshless method, Journal of Sound and Vibration 319 (2009) 984–992.
[15] Ferreira AJM, Batra RC. Natural frequenciesof orthotropic, monoclinic and hexagonal plates by a meshless method, Journal of Sound and Vibration 285 (2005) 734–742.
[16] Wu YC, Yang Q, Kong X, Zhi P, Xiao J. Uncertainty quantification for the representative volume element of geometrically monoclinic 3D printed concrete, Int. J. Solids Struct. 226-227 (2021) 111102.
[17] Oxman N, Tsai E, Firstenberg M. Digital anisotropy: A variable elasticity rapid prototyping platform [J].Virtual and Physical Prototyping,2012,7(4):261-274.
[18] Ma G, Li Z, Wang L, Wang F, Sanjayan J. Mechanical anisotropy of aligned fiber reinforced composite for extrusion-based 3D printing, Const. and Build. Mater. 202 (2019) 770-783.
[19] Ma G, Zhang J, Wang L, Li Z, Sun J. Mechanical characterization of 3D printed anisotropic cementitious material by the electromechanical transducer, Smart Mater. Struc. 27 (2018) 075036.
[20] Xiao J, Liu H, Ding T. Finite element analysis on the anisotropic behavior of 3D printed concrete under compression and flexure[J]. Additive Manufacturing, 2021, 39
[21] Reiter L, Wangler T, Roussel N, et al. The role of early age structural build-up in digital fabrication with concrete. Cem Concr Res 2018;112:86–95.
[22] Wolfs RJM, Bos FP, Salet TAM. Hardened properties of 3D printed concrete: the influence of process parameters on interlayer adhesion. Cem Concr Res 2019;119:132–40.
[23] T. Hughes, J. Cottrell, Y. Bazilevs, Isogeometric analysis: CAD, finite elements, NURBS, exact geometry and mesh refinement, Comput. Methods Appl. Mech. Engrg. 194 (2005) 4135–4195.
[24] Cottrell J A, Reali A, Bazilevs Y, Hughes T J R.Isogeometric analysis of structural vibrations [J].Computer Methods in Applied Mechanics andEngineering, 2006, 195(41/42/43): 5257－5296.
[25] Al Abadi H, Thai HT, Paton-Cole V, et al. Elastic properties of 3D printed fibrereinforced structures. Compos Struct 2018;193:8–18.